NANO LETTERS
2009
Vol. 9, No. 9
3214-3219

Lateral Buckling Mechanics in Silicon Nanowires on Elastomeric Substrates

Seung Yoon Ryu,[†] Jianliang Xiao,[‡] Won Il Park,[†] Kwang Soo Son,[†] Yonggang Y. Huang,[*,‡] Ungyu Paik,[*,†] and John A. Rogers[*,§]

Division of Materials Science Engineering, Hanyang University, 17 Haengdang-dong, Seongdong-gu, Seoul 133-791, Republic of Korea, Departments of Civil and Environmental Engineering and Mechanical Engineering, Northwestern University, Evanston, Illinois 60208, and Department of Materials Science and Engineering, Department of Mechanical Science and Engineering, Department of Physics, Beckman Institute, Frederick-Seitz Materials Research Laboratory, University of Illinois at Urbana−Champaign, Illinois 61801

Received May 6, 2009; Revised Manuscript Received July 17, 2009

ABSTRACT

We describe experimental and theoretical studies of the buckling mechanics in silicon nanowires (SiNWs) on elastomeric substrates. The system involves randomly oriented SiNWs grown using established procedures on silicon wafers, and then transferred and organized into aligned arrays on prestrained slabs of poly(dimethylsiloxane) (PDMS). Releasing the prestrain leads to nonlinear mechanical buckling processes that transform the initially linear SiNWs into sinusoidal (i.e., "wavy") shapes. The displacements associated with these waves lie in the plane of the substrate, unlike previously observed behavior in analogous systems of silicon nanoribbons and carbon nanotubes where motion occurs out-of-plane. Theoretical analysis indicates that the energy associated with this in-plane buckling is slightly lower than the out-of-plane case for the geometries and mechanical properties that characterize the SiNWs. An accurate measurement of the Young's modulus of individual SiNWs, between ∼170 and ∼110 GPa for the range of wires examined here, emerges from comparison of theoretical analysis to experimental observations. A simple strain gauge built using SiNWs in these wavy geometries demonstrates one area of potential application.

Recent work demonstrates that controlled mechanical buckling processes[1−7] can be exploited in fields ranging from thin film metrology[8] to stretchable electronics[9−13] and biotechnology.[14] For electronics, inorganic semiconductor nanoribbon active materials can be transfer printed, using stamps of polydimethylsiloxane (PDMS),[15,16] from a source wafer to a PDMS substrate where they adopt buckled, or wavy configurations. In such forms, they can be stretched and compressed in a nondestructive way with a physics that is related to the motion of an accordion bellows. Similar concepts can be applied to aligned arrays of single-wall carbon nanotubes (SWNTs),[5] not only to yield stretchable nanotube devices but also to infer their intrinsic, linear elastic mechanical properties in an accurate and statistically significant manner.[5] Related manipulation of silicon nanowires (SiNWs),[17−20] which represent an attractive material for macro-, micro-, and nanoelectronics[21,22] and ultrasensitive sensors for chemical and biological detection,[23,24] is therefore of some interest. Here, we demonstrate the mechanics of buckling of arrays of SiNWs, formed by vapor−liquid−solid (VLS) growth and transferred onto PDMS substrates. The behavior involves lateral buckling configurations that have not been observed in previous studies of other nanostructures.[1−7] Analysis by theoretical modeling explains these results and enables accurate determination of the Young's modulus of individual wires from measurements of their dimensions and buckling geometries. A simple strain gauge demonstrates one possible application of wavy SiNWs.

Figure 1 provides a schematic illustration of the fabrication process. SiNWs were prepared on Si substrates using Au nanoclusters as catalysts in a conventional VLS process (Figure 1a). A contact printing method applied to these SiNWs yielded highly ordered and aligned arrays of linear wires.[25−28] This process involved rubbing the growth (i.e., donor) substrate onto a receiver substrate under an applied load, as shown in Figure 1b,c.[27,28] Aligned SiNWs formed in this manner were transferred to a prestrained PDMS slab by transfer printing,[29] with some uniaxial tensile force applied along the lengths of the wires. Total prestrain involves the combined effects of applied prestrain and strain associated with transfer. Figure 1f shows a large area optical micrograph. We observe that >60% of the wires show buckled structures, distributed uniformly over the sample. The

* To whom correspondence should be addressed. E-mail: (U.P.) upaik@hanyang.ac.kr; (Y.Y.H.) y-huang@northwestern.edu; (J.A.R.) jrogers@ad.uiuc.edu.
[†] Hanyang University.
[‡] Northwestern University.
[§] University of Illinois at Urbana−Champaign.

10.1021/nl901450q CCC: $40.75
Published on Web 08/11/2009

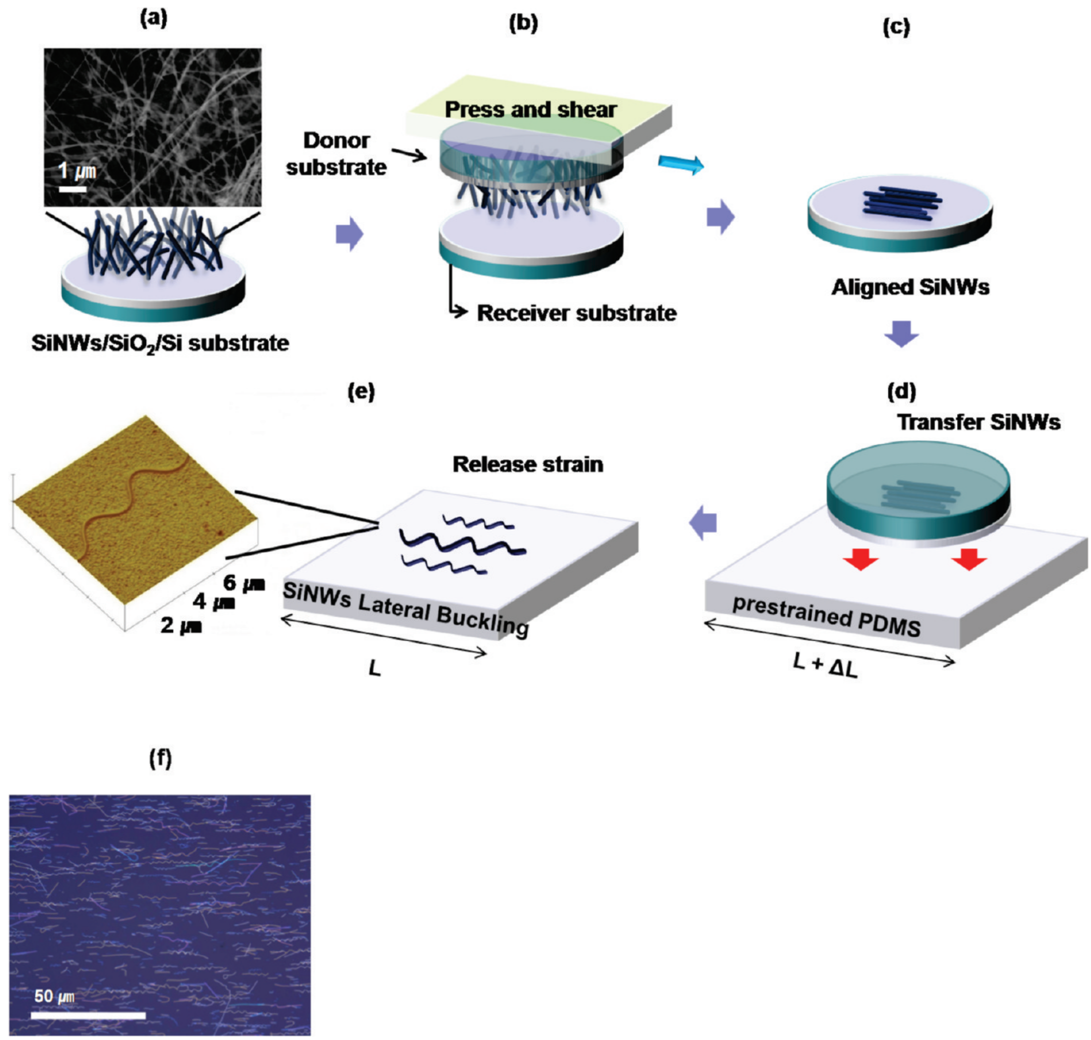

Figure 1. Schematic illustration of the process for forming wavy, buckled SiNWs by first transferring wires grown on a silicon wafer to a receiver substrate and then to a prestrained slab of PDMS, followed by release of the prestrain. (a) Randomly oriented collection of SiNWs formed by VLS growth on a substrate of SiO_2 (300 nm)/Si. (b) Rubbing this wafer against a receiver substrate under a weight leads to the formation of aligned arrays of linear SiNWs. (c) Well-aligned SiNW array on the receiver. (d) Transfer printing delivers these aligned SiNWs to a PDMS substrate under prestrain. (e) Releasing this prestrain induces compressive strains on the SiNWs that cause them to buckle laterally, thereby adopting "wavy" shapes in the plane of the PDMS surface. (f) A large area optical micrograph.

unbuckled wires are typically either (1) poorly aligned with the direction of prestrain due to imperfections in the transfer/orientation process or (2) shorter than the characteristic length (between 2 and 7 μm for the wires reported here) over which the amplitudes of the buckled structures decay toward the ends of the wires (as defined by the mechanics[30]). Releasing the prestrain yielded laterally buckled SiNWs as observed by atomic force microscope (AFM) and field-emission scanning electron microscope (FE-SEM) images (Figure 2). These results show that the SiNWs remain on the surface of the PDMS and that the buckling is lateral, that is, there is very little surface relief associated with these deformations. As described in detail below, good agreement between mechanics models that assume no slipping of the nanowires on the substrate provide some evidence for strong adhesion. This deformation mode is different from that observed previously in ribbons, membranes, and carbon nanotubes in otherwise similar systems. The heights of the SiNWs were between 40 and 170 nm, implying radii between 20 and 85 nm. The wavelengths of the lateral buckling structures were between 2000 and 7000 nm. Figure 2b shows an FE-SEM image of a SiNW transferred to an unstrained PDMS substrate. Figure 2c−e shows some representative cases when prestrain is involved. From analysis of the contour shape, we infer maximum strains in the silicon of <6% for all cases examined. This strain is somewhat smaller than the fracture strain of SiNWs reported previously.[31] At sufficiently high prestrain, it may be possible to use these methods to examine systematically ultimate strength and failure in the wires.

Analysis of FE-SEM images yielded wavelengths and radii of individual buckled SiNWs, Figure 2c corresponds to a SiNW with a radius of 20∼30 nm, a wavelength of 2500∼3500 nm, and an amplitude of 400∼600 nm with a total of ∼ 10 wavelengths. Figure 2d,e shows SiNWs with radii of 40∼50 nm, wavelengths of ∼4000 nm, and amplitudes of 600∼800 nm. Analysis of many SiNWs on a single substrate reveals an approximately linear increase of the wavelength and amplitude with radius (Figure 3). All of these phenomena can be explained by a Newtonian analytical mechanics model based on linear elasticity theory. Previous

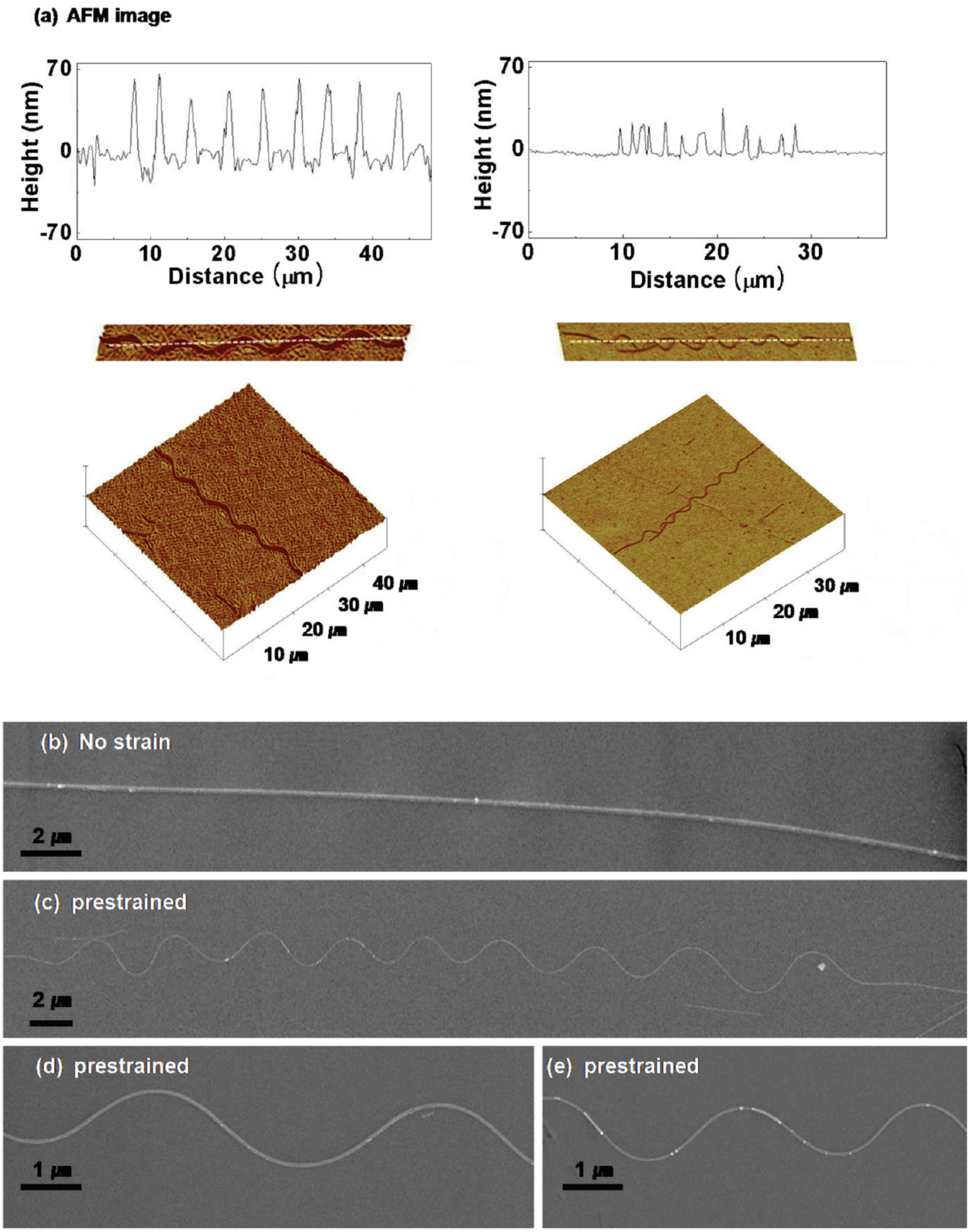

Figure 2. AFM and FE-SEM images of lateral buckling of SiNWs on a PDMS substrate. (a) AFM images of two representative cases, showing an absence of any significant out of plane displacement associated with the buckling. (b) FE-SEM image of a SiNW on a PDMS substrate without the use of any prestrain. The absence of buckling indicates the critical role of the prestrain in this process. (c) FE-SEM image of a thin and long SiNW buckled with ~10 wavelengths. (d,e) FE-SEM images of comparatively thick, buckled wires.

experimental reports of SiNWs formed by VLS and well computer simulation suggest that [111] is the growth direction and that the wires have hexagonal cross sections, consistent with the Stillinger−Weber (SW) potential method.[20,25,26,33] For a SiNW with a hexagonal cross section of outer radius R, the cross sectional area is $S = (3\sqrt{3}/2)R^2$ and the moment of inertia is $I = (5\sqrt{3}/16)R^4$. For the experiments reported here, such a wire can be modeled as an elastic beam with bending stiffness $E_{SiNW}I$ and tensile stiffness $E_{SiNW}S$ since the radii R (~50 nm) are much smaller than the buckling wavelengths (~5000 nm), where E_{SiNW} is the Young's modulus of SiNW. In the following, the PDMS substrate is treated as a semi-infinite solid (i.e., its thickness is orders of magnitude larger than the other length scales) of Young's modulus E_S and Poisson's ratio $\nu_S \approx 0.5$. We assume that the in-plane displacement of the buckled SiNW takes a sinusoidal form $w = A\cos(kx)$ with amplitude A and wave vector $\mathbf{k}$. (The wavelength is $\lambda = 2\pi/\mathbf{k}$.) The total system energy is composed of three parts, the strain energy in the PDMS substrate (U_S), the membrane and bending energies of the SiNW ($U_{membrane}$ and $U_{bending}$), the analytical expressions of which are obtained as $U_S = \{[(5 - 2\gamma - 2$

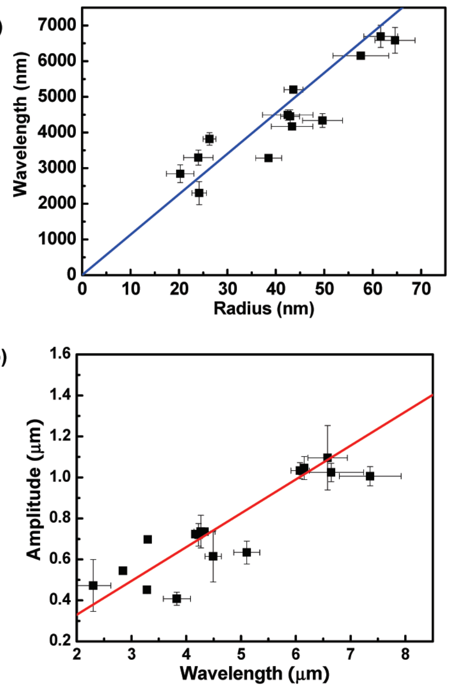

Figure 3. Experimental (symbols) and theoretical (lines) results for the dependence of the buckling wavelength and amplitude on radii of the SiNWs. (a) Comparison of measured (symbols) and computed (lines; linear fit with one fitting parameter) variation of buckling wavelength with radius. The fitting yields an average Young's modulus for this set of wires of ~140 GPa. (b) Comparison of measured (symbols) and computed (lines; no fitting parameters)) variation of buckling amplitude with radius. The good agreement validates the modeling and experimental approach.

$\ln \mathbf{k}R)]/(4\pi\bar{E}_S)\}[(E_{SiNW}I)A\mathbf{k}^4 + (E_{SiNW}S)A\mathbf{k}^2((1/4)\mathbf{k}^2A^2 - \varepsilon_{pre})]^2$, $U_{membrane} = [(E_{SiNW}S)/2][(1/4)\mathbf{k}^2A^2 - \varepsilon_{pre})^2]$ and $U_{bending} = (1/4)E_{SiNW}IA^2\mathbf{k}^4$, respectively, where $\gamma = 0.577$ is Euler's constant, $\bar{E}_S = E_S/(1 - \nu_S^2)$ is the plane-strain modulus of the PDMS substrate, and ε_{pre} is the prestrain. Minimizing the total system energy with respect to A and $\mathbf{k}$ gives the expressions for the wave vector and amplitude as[34]

$$\left(\frac{E_{SiNW}I}{\bar{E}_S}\right)^{1/4} k = \left[\frac{2\pi(2 + \ln 2 - \gamma - \ln \mathbf{k}R)}{(5 + 2\ln 2 - 2\gamma - 2\ln \mathbf{k}R)^2}\right]^{1/4} \quad (1)$$

$$A = \frac{2}{\mathbf{k}}\left(\varepsilon_{pre} - \frac{E_{SiNW}I}{E_{SiNW}S}k^2 - \frac{\pi\bar{E}_S}{E_{SiNW}S\mathbf{k}^2}\frac{1}{5 + 2\ln 2 - 2\gamma - 2\ln \mathbf{k}R}\right)^{1/2} \quad (2)$$

The solution of eq 1 is

$$\mathbf{k}R = C \approx \frac{5}{6}\left(\frac{\bar{E}_S}{E_{SiNW}}\right)^{1/4}, \text{ or } \quad \lambda \approx \frac{12\pi}{5}\left(\frac{E_{SiNW}}{\bar{E}_S}\right)^{1/4} R \quad (3)$$

where C depends only on the modulus ratio $\bar{E}_S/E_{SiNW}$ of PDMS substrate and SiNW. The buckle amplitude is then given by

$$A = \frac{2R}{C}\sqrt{\varepsilon_{pre} - \varepsilon_{critical}} \approx \frac{12}{5}\left(\frac{E_{SiNW}}{\bar{E}_S}\right)^{1/4} R\sqrt{\varepsilon_{pre} - \varepsilon_{critical}} \quad (4)$$

which is linearly proportional to the SiNW radius R, where $\varepsilon_{critical}$ is the critical prestrain for buckling and is given by

$$\varepsilon_{critical} = \frac{5}{24}C^2 + \frac{2\sqrt{3}\pi\bar{E}_S}{9C^2E_{SiNW}}\frac{1}{5 + 2\ln 2 - 2\gamma - 2\ln C} \approx \frac{3}{10}\left(\frac{\bar{E}_S}{E_{SiNW}}\right)^{1/2} \quad (5)$$

which depends only on the ratio of substrate/SiNW Young's moduli.

The fit of measured wavelengths and radii by the linear relation in eq 3 gives $C = 0.055 \pm 0.003$ as shown in Figure 3a. For the Young's modulus of PDMS $E_S = 2$ MPa[35] (plane-strain modulus $\bar{E}_S = 2.67$ MPa), this value of C implies $E_{SiNW} = 140 \pm 30$ GPa. Although the modulus could conceivably vary with diameter,[32] our model assumes a diameter independent value, consistent with the measured data to within experimental uncertainties. For wires with diameters in the range studied here, a native oxide layer has negligible influence on the mechanics. This result corresponds well with literature reports of moduli of silicon in bulk, ribbon, polycrystalline, amorphous, and nanowire forms, 163−188 GPa,[36,37] 160 GPa,[38] 149−171 GPa,[39,40] 124 GPa,[41] and 94.4−175 GPa,[17−19] respectively. We also find quantitative agreement between measurements and modeling of the dependence of the amplitude on radius, as illustrated in Figure 3b, where $A = \lambda(\varepsilon_{pre} - \varepsilon_{critical})^{1/2}/\pi$ is obtained from eqs 3 and 4, and ε_{pre} is determined from the measured contour $\lambda_{contour}$ and buckling wavelength λ as $\varepsilon_{pre} = \ln(\lambda_{contour}/\lambda)$.[35]

Prior studies of single walled carbon nanotubes (SWNTs) in otherwise similar systems showed predominantly out-of-plane (normal) buckling behavior,[5,34] as opposed to the in-plane (lateral) geometries observed here in SiNWs. To investigate this issue, we computed the total system energies for out-of-plane (normal)[34] and in-plane (lateral) buckling of SiNWs on prestrained PDMS substrate, and plotted the results in Figure 4, with $E_{(SiNW)} = 137$ GPa and $\bar{E}_S = 2.67$ MPa. Lateral buckling gives slightly lower energy and is therefore more energetically favorable than normal buckling; this result provides an explanation for lateral buckling in SiNWs. For example, a SiNW of radius 50 nm has energies of 33.9 and 37.6 nJ/m for lateral and normal buckling, respectively. The energy difference 3.7 nJ/m (~10% difference) for the one-dimensional SiNW is significant since it corresponds to 74 mJ/m^2 (3.7 nJ/m divided by the diameter 50 nm) in 2D, which is almost 50% larger than the adhesion energy between Si and PDMS (50.6 mJ/m^2). We speculate that the normal mode buckling associated with SWNTs results from lateral constraints provided by surface roughness (~1 nm) on the PDMS, which is comparable to or larger than the radii of the SWNTs but is negligible for the SiNWs.

As a device application of wavy SiNWs, Figure 5 shows a simple strain gauge demonstrator involving electrical

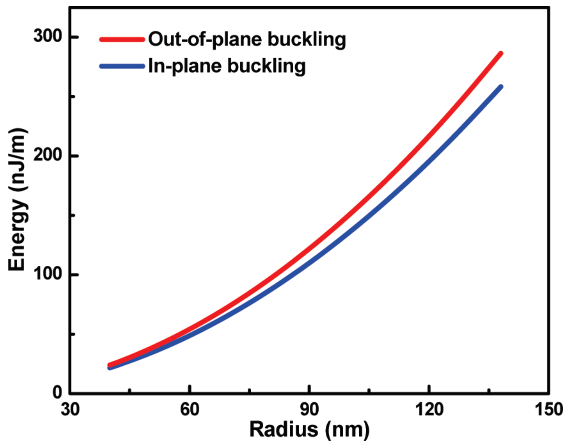

Figure 4. The total system energy for out-of-plane and in-plane buckling for the case of SiNWs on a PDMS substrate. Here, $E_{(\mathrm{SiNW})} = 137$ GPa and $\bar{E}_S = 2.67$ MPa. The slightly lower energy for the in-plane case favors this buckling mode.

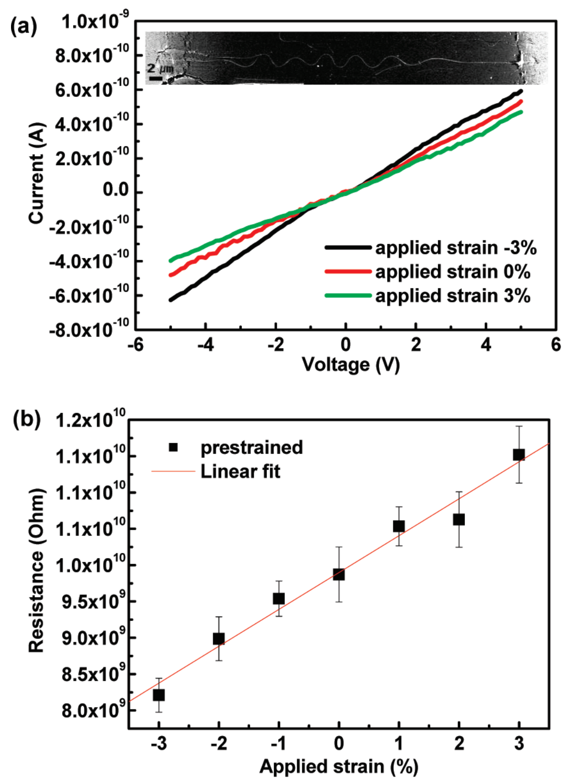

Figure 5. Simple strain gauge device using a buckled SiNW. (a) Current vs voltage plot from a device with gold electrodes (100 nm) and a single SiNWs. The inset shows an FE-SEM image for a SiNW connected to electrodes. (b) Device resistance as a function of applied strain. The gauge factor is ~5.6.

contacts to wavy SiNWs (formed in procedures like those described previously). The plot presents current−voltage characteristics of a device with 100 nm thick gold electrodes formed by thermal evaporation through a shadow mask having a gap of ~60 μm between electrodes. Immediately prior to forming these electrodes, the SiNWs on PDMS were dipped briefly hydrofluoric acid (volume percent 10%) to remove the native oxide for the purpose of improving the electrical contacts. A typical device involved a single wavy SiNW, as confirmed by FE-SEM images such as the one in the inset of Figure 5a. We suspect that the relatively low current levels resulted from poor contacts, which we could not thermally anneal due to the use of PDMS as the substrate. An effective resistance was measured using Ohm's law and linear fitting from −5 to 5 V. This resistance changed systematically with applied strain, as shown in Figure 5b, with a behavior that can be described empirically using a piezoresistance gauge factor (GF), defined as GF $=(\Delta R/R)/\Delta\varepsilon_a$, where R and ΔR indicate the resistance and change in resistance with a change in applied strain $\Delta\varepsilon_a$.[5] Although the buckled configuration for strain sensing has the disadvantage that compressive and tensile stresses are partially balanced, a gauge of this type can provide measurements of smaller forces and for larger displacements than would be possible in unbuckled geometries. A typical GF value in this study was ~5.6 with a total range of 4.8 and 6.7 for each sample. The change in the resistance of the electrode were in all cases negligible throughout the strain range examined experimentally. The GF values observed in the wavy SiNWs devices are smaller than other reports of silicon in various forms, likely because the wavy geometry involves balanced compressive and tensile strains for any applied strain (less than the prestrain). For example, the piezoresistance coefficients of straight SiNWs lie between ~1000 and ~3000,[42] having the diameters of ~90 nm in SiNWs with a strong size dependence in which, in a separate report, the GF varies from 32 to 1547[43] for wire diameters from 50 to 350 nm. By comparison, the GF of gated hydrogenated amorphous silicon[44] and bulk silicon[45,46] are ~2.4 and 50−150, respectively.

In conclusion, the studies presented here represent the first observations of nonlinear buckling mechanics in SiNWs. The results show lateral buckled geometries that are quantitatively in agreement with analytical models for the mechanics. The experimental procedures and theoretical analysis approaches provide experimentally simple routes to measuring the linear elastic properties of nanowire materials in general. Viewed in another manner, they also suggest a path to stretchable nanowire electronics/sensors, as suggested by our strain gauge device. Both areas offer many opportunities for additional research.

Acknowledgment. This work was financially supported by National Research Foundation of Korea (NRF) through a Grant (K2070400000307A050000310, Global Research Laboratory (GRL) Program) provided by the Korean Ministry of Education, Science, and Technology (MEST) in 2009.

References

(1) Nolte, A. J.; Rubner, M. F.; Cohen, R. E. *Macromolecules* **2005**, *38*, 5367–5370.
(2) Sun, Y.; Kumar, V.; Adesida, I.; Rogers, J. A. *Adv. Mater.* **2006**, *18*, 2857–2862.
(3) Sun, Y.; Choi, W. M.; Jiang, H.; Huang, Y. Y.; Rogers, J. A. *Nat. Nanotechnol.* **2006**, *1*, 201–207.
(4) Sun, Y.; Rogers, J. A. *J. Mater. Chem.* **2007**, *17*, 832–840.

(5) Khang, D. -Y.; Xiao, J.; Kocabas, C.; MacLaren, S.; Banks, T.; Jiang, H.; Huang, Y. Y.; Rogers, J. A. *Nano Lett.* **2008**, *8*, 124–130.

(6) Jiang, H.; Khang, D. -Y.; Fei, H.; Kim, H.; Huang, Y.; Xiao, J.; Rogers, J. A. *J. Mech. Phys. Solids* **2008**, *56*, 2585–2598.

(7) Khang, D. -Y.; Rogers, J. A.; Lee, H. H. *Adv. Funct. Mater.* **2008**, *18*, 1–11.

(8) Stafford, C. M.; Harrison, C.; Beers, K. L.; Karim, A.; Amis, E. J.; Vanlandingham, M. R.; Kim, H. -C.; Volksen, W.; Miller, R. D.; Simonyi, E. E. *Nat. Mater.* **2004**, *3*, 545–550.

(9) Khang, D. -Y.; Jiang, H.; Huang, Y.; Rogers, J. A. *Science* **2006**, *311*, 208–212.

(10) Kim, D. -H.; Ahn, J. -H.; Choi, W. M.; Kim, H. -S.; Kim, T. -H.; Song, J.; Huang, Y. Y.; Liu, Z.; Lu, C.; Rogers, J. A. *Science* **2008**, *320*, 507–511.

(11) Ko, H. C.; Stoykovich, M. P.; Song, J.; Malyarchuk, V.; Choi, W. M.; Yu, C. -J.; Geddes III, J. B.; Xiao, J.; Wang, S.; Huang, Y.; Rogers, J. A. *Nature* **2008**, *454*, 748–753.

(12) Kim, D. -H.; Song, J.; Choi, W. M.; Kim, H. -S.; Kim, R. -H.; Liu, Z.; Huang, Y. Y.; Hwang, K. -C.; Zhang, Y; Rogers, J. A. *Proc. Natl. Acad. Sci. U.S.A.* **2008**, *105*, 18675–18680.

(13) Kim, D. -H.; Rogers, J. A. *Adv. Mater.* **2008**, *20*, 1–6.

(14) Efimenko, K.; Rackaitis, M.; Manias, E.; Vaziri, A.; Mahadevan, L.; Genzer, J. *Nat. Mater.* **2005**, *4*, 293–297.

(15) Ferguson, G. S.; Chaudhury, M. K.; Sigal, G. B.; Whitesides, G. M. *Science* **1991**, *253*, 776–778.

(16) Bowden, N.; Brittain, S.; Evans, A. G.; Hutchinson, J. W.; Whitesides, G. M. *Nature* **1998**, *393*, 146–149.

(17) Menon, M.; Srivastava, D.; Ponomareva, I.; Chernozatonskii, L. A. *Phys. Rev. B* **2004**, *70*, 125313/1–125313/6.

(18) Li, Q.; Koo, S. -M.; Edelstein, M. D.; Suehle, J. S.; Richter, C. A. *Nanotechnology* **2007**, *18*, 315202/1–315202/5.

(19) Hsin, C.-L.; Mai, W.; Gu, Y.; Gao, Y.; Huang, C.-T.; Liu, Y.; Chen, L.-J.; Wang, Z.-L. *Adv. Mater.* **2008**, *20*, 1–5.

(20) Jing, Y.; Meng, Q.; Gao, Y. *Comput. Mater. Sci.* **2009**, *45*, 321–326.

(21) Cui, Y.; Lieber, C. M. *Science* **2001**, *291*, 851–853.

(22) Feng, X. L.; He, R.; Yang, P.; Roukes, M. L. *Nano Lett.* **2007**, *7*, 1953–1959.

(23) Cui, Y.; Wei, Q.; Park, H.; Lieber, C. M. *Science* **2001**, *293*, 1289–1292.

(24) Su, S.; He, Y.; Zhang, M.; Yang, K.; Song, S.; Zhang, X.; Fan, C.; Lee, S.-T. *Appl. Phys. Lett.* **2008**, *93*, 023113/1–023113/3.

(25) Cui, Y.; Lauhon, L. J.; Gudiksen, M. S.; Wang, J.; Lieber, C. M. *Appl. Phys. Lett.* **2001**, *78*, 2214–2216.

(26) Wu, Y.; Cui, Y.; Huynh, L.; Barrelet, C. J.; Bell, D. C.; Lieber, C. M. *Nano Lett.* **2004**, *4*, 433–436.

(27) Javey, A.; Nam, S. W.; Friedman, R. S.; Yan, H.; Lieber, C. M. *Nano Lett.* **2007**, *7*, 773–777.

(28) Fan, Z.; Ho, J. C.; Jacobson, Z. A.; Yerushalmi, R.; Alley, R. L.; Razavi, H.; Javey, A. *Nano Lett.* **2008**, *8*, 20–25.

(29) Meitl, M. A.; Zhu, Z. -T.; Kumar, V.; Lee, K. J.; Feng, X.; Huang, Y. Y.; Adesida, I.; Nuzzo, R. G.; Rogers, J. A. *Nat. Mater.* **2006**, *5*, 33–38.

(30) Koh, C. T.; Liu, Z. J.; Khang, D.-Y.; Song, J.; Lu, C.; Huang, Y.; Rogers, J. A.; Koh, C. G. *Appl. Phys. Lett.* **2007**, *91*, 133113/1–133113/3.

(31) Hoffmann, S.; Utke, I.; Moser, B.; Michler, J.; Christiansen, S. H.; Shmidt, V.; Senz, S.; Werner, P.; Gösele, U.; Ballif, C. *Nano Lett.* **2006**, *6*, 622–625.

(32) Huang, H.; Swygenhoven, H. V. *MRS Bull.* **2009**, *34*, 160–166.

(33) Lee, B.; Rudd, R. E. *Phys. Rev. B* **2007**, *75*, 041305/1–041305/4.

(34) Xiao, J.; Jiang, H.; Khang, D.-Y.; Wu, J.; Huang, Y.; Rogers, J. A. *J. Appl. Phys.* **2008**, *104*, 033543/1–033543/7.

(35) Choi, K. M.; Rogers, J. A. *J. Am. Chem. Soc.* **2003**, *125*, 4060–4061.

(36) Dolbow, J.; Gosz, M. *Mech. Mater.* **1996**, *23*, 311–321.

(37) Kim, M. T. *Thin Solid Films* **1996**, *283*, 12–16.

(38) Baca, A. J.; Meitl, M. A.; Ko, H. C.; Mack, S.; Kim, H. -S.; Dong, J.; Ferreira, P. M.; Rogers, J. A. *Adv. Funct. Mater.* **2007**, *17*, 3051–3062.

(39) Cho, S. W.; Chasiotis, I. *Exp. Mech.* **2007**, *47*, 37–49.

(40) Maier-Schneider, D.; Köprülülü, A.; Holm, S. B.; Obermeier, E. *J. Micromech. Microeng.* **1996**, *6*, 436–446.

(41) Mathioudakis, C.; Kelires, P. C. *J. Non-Cryst. Solids* **2000**, *266−269*, 161–165.

(42) He, R.; Yang, P. *Nat. Nanotechnol.* **2006**, *1*, 42–46.

(43) Reck, K.; Richter, J.; Hausen, O.; Thomsen, E. V. *Proc. IEEE MEMS* **2008**, 717–720.

(44) Zhou, L.; Jung, S.; Brandon, E.; Jackson, T. N. *IEEE Trans. Electron Devices* **2006**, *53*, 380–385.

(45) Rowe, A. C. H.; Donoso-Barrera, A.; Renner, Ch.; Arscott, S. *Phys. Rev. Lett.* **2008**, *100*, 145501/1–145501/4.

(46) Villanueva, G.; Plaza, J. A.; Montserrat, J.; Perez-Murano, F.; Bausells, J. *Microelectron. Eng.* **2008**, *85*, 1120–1123.

NL901450Q